Laser-excited PEEM using a fully tunable fs-laser system

A. Höfer
K. Duncker
M. Kiel
S. Förster
W. Widdra

The ferroelectric domain structure on a (001) surface of a $BaTiO_3$ single crystal prepared under ultrahigh vacuum conditions is imaged by laser-excited photoemission electron microscopy (PEEM). The PEEM images allow for discrimination of three domain types by their different photoemission yields. To characterize the contrast between the different ferroelectric domains of $BaTiO_3$(001) in the region of 4.0–4.6 eV close to the photoemission threshold, the broad wavelength tunability of the femtosecond laser system is used. The femtosecond time resolution within two-photon PEEM experiments, using two fully independently tunable laser beams, is demonstrated for the first image potential state of Ag(001). In a pump-probe setup with a cross-correlation full-width at half-maximum of 70 fs, an angle-integrated apparent lifetime of 40 fs is derived from the PEEM intensities. In contrast with energy-resolved two-photon photoemission measurements, PEEM data reveal a 17-fs shorter lifetime. This difference is discussed by considering the co-excitation of bulk states, which leads to an additional time-dependent photoelectron contribution in PEEM.

Introduction

Photoelectrons emitted from a crystal surface give access to the energy-resolved density of states and the electronic band structure. This correlation is widely used in spatially averaging methods such as ultraviolet photoelectron spectroscopy. In contrast, photoemission electron microscopy (PEEM) yields the 2-D distribution of the photoelectrons with a spatial resolution in the nanometer range in state-of-the-art instruments. The direct imaging by electron optics as realized in PEEM enables fast image acquisition since it avoids sequential scanning of the sample as in scanning probe techniques. The electronic contrast accessible to PEEM depends significantly on the photon energy used for sample illumination. For laboratory use, PEEM is often combined with an ultraviolet gas discharge lamp (Hg, He) with a characteristic fixed spectrum. It gives access to the occupied valence states close to the Fermi energy, revealing a high contrast for small variations in the work function (threshold PEEM). In contrast, X-ray synchrotron radiation allows for excitation of core-level electrons, leading to high element specificity. By the use of X-ray circular magnetic dichroism (XMCD), magnetic domain contrast is also possible [1]. The utilization of femtosecond (fs) lasers for sample illumination in PEEM gives access to the unoccupied electronic states by multiphoton photoemission and creates the possibility to directly image the fs dynamics at surfaces in time-resolved pump-probe experiments [2, 3]. Since the first time-resolved two-photon PEEM (2P-PEEM) experiments, this technique has been applied to manifold surface science problems. Several studies have addressed the surface plasmon propagation directly in and in the vicinity of differently shaped metal nanostructures [4–8]. Quite recently, energy-resolved 2P-PEEM measurements have been demonstrated for the first time [9, 10]. Aside from these pure laser pump-probe experiments, combinations with synchrotron X-rays have also been developed to obtain access to the temporal evolution of magnetic structures [11, 12]. Apart from the excellent temporal resolution of laser light, the adjustable polarization is also used for magnetic linear and magnetic circular dichroism contrast of magnetic surfaces [13, 14].

In most experiments, the light of a pulsed Ti:Sapphire laser or its higher harmonics is used for photoemission, which results in a limited range of possible photon energies. With a carefully chosen sample or by additional exposure to alkali metals (to lower the sample work function), this allows the performance of threshold laser-excited PEEM (e.g., [15, 16]). In this paper, we present a laser-excited PEEM study with a

Digital Object Identifier: 10.1147/JRD.2011.2156210

0018-8646/11/$5.00 © 2011 IBM

highly versatile high-repetition-rate laser setup that enables photoexcitation over a wide range of photon energies. The laser tunability is used for microscopy of the photoemission onset in one-photon PEEM experiments of a ferroelectric surface, whereas two-photon ultraviolet and infrared (UV+IR) PEEM experiments demonstrate an excellent time resolution in pump-probe experiments.

Since the discovery of the ferroelectric properties of $BaTiO_3$ in the 1940s, its ferroelectric domain structure in ceramics and crystals has been studied intensively [17, 18]. $BaTiO_3$ has a perovskite structure that is temperature dependent with different phases [19]. The equilibrium phase between 275 and 400 K shows a tetragonal symmetry accompanied by a relative shift between the positively and negatively charged ions along the crystallographic *c*-axis, which leads to its ferroelectric behavior. In contrast to ferromagnetism, the resulting electric polarization is always oriented along one of the ⟨100⟩ directions of the crystal. This strict coupling to the crystallographic axes is due to the large anisotropy energy [20]. Therefore, three different ferroelectric domain types can be discriminated on the (001) surface, depending on the direction of the polarization relative to the surface normal. In many early studies, experiments have been carried out under ambient conditions that make a selective surface preparation redundant, and the adsorption of screening charges is inevitable. In the early 1970s, Le Bihan et al. showed that the ferroelectric domains of $BaTiO_3$ lead to a photoemission contrast in PEEM [21]. For these measurements, the samples were polished or bombarded by Ar^+ ions without a special ultrahigh vacuum (UHV) treatment. Only more recently, the surface properties of $BaTiO_3$ have been studied under UHV conditions in more detail [22, 23].

As depicted schematically in **Figure 1** (upper portion), the domain structure of the (001) surface of a $BaTiO_3$ crystal, for which the electric polarization is parallel to the surface normal, leads to either the c^+ or the c^- domains, depending on the polarization orientation. Additionally, four different *a* domains can form for which the polarization is oriented perpendicular to the surface normal. As indicated in the upper portion of Figure 1, the 90° *a*–*c* domain walls coincide with the (110) crystal planes and tend to align straight with the high symmetry directions of the crystal. In contrast, the 180° domain walls are less sensitive to crystallographic directions and are more or less arbitrarily shaped [24]. In the c^+ and c^- domains, the spontaneous polarization of the unit cell leads to an accumulation of positive and negative charges, respectively, close to the surface, whereas no charge accumulation takes place there for the *a* domains. The resulting surface potential is schematically shown in the lower portion of Figure 1. It is lowered for the c^+ domains and increased for the c^- domains with respect to the *a*-domain potential, as derived from evaluation of the Poisson equation. For a more elaborated discussion, one has to take into account that the positions of the Fermi and the vacuum level, as well as the energy-dependent density of states, also depend on the polarization direction [25]. Based on both approaches, shifted photoemission onsets and different photoemission intensities for the three domains are expected, which might lead to a strong PEEM contrast in threshold measurements, as shown in this paper.

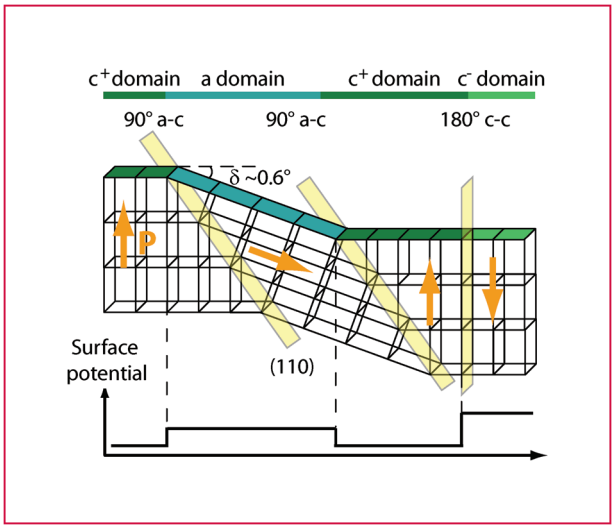

Figure 1

Domain structure and surface potential. (top of figure) Sketch of three different ferroelectric domain types present at a $BaTiO_3(001)$ surface (side view). Note the small angle δ in surface topography at a domain wall between in-plane and out-of-plane domains, *a* and *c*, respectively. (lower part of figure) Schematic diagram of the surface potential of the different domains caused by the polarization-dependent charge accumulation close to the surface.

Experiment

The setup for laser-excited and time-resolved PEEM experiments is depicted in **Figure 2**. The laser system consists of two main parts, i.e., an all-fiber pump laser (IMPULSE**; Clark-MXR, Inc., Dexter, MI, USA) and a noncollinear optical parametric amplifier (NOPA, i-NOPA** duo; Clark-MXR). The pump laser follows a novel oscillator concept, in which an Yb-doped fiber is directly pumped by a continuous-wave laser diode, generating laser pulses at a central wavelength of 1,035 nm with a repetition rate of 25 MHz. After adequate pulse picking in the range of 200 kHz to 2 MHz, the resulting laser pulses are amplified within three sequential fibers to pulse energies of 10 μJ. In the present experiments, this output drives at a repetition rate of 1.5 MHz simultaneously two independent NOPAs, as developed by Homann et al. [26].

To summarize, in the i-NOPA duo, the 1,035-nm fundamental beam is split into two parts, where one part passes a sapphire disk for white light continuum generation

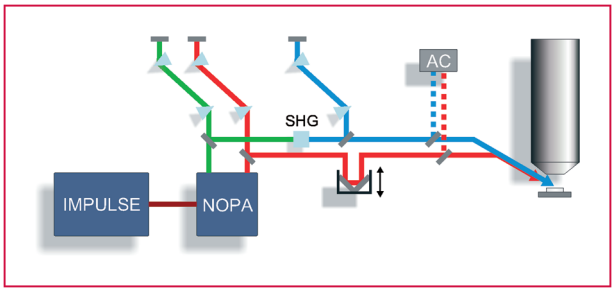

Figure 2

Schematics of the time-resolved, two-color photoemission experiment. A fiber laser drives two noncollinear optical parametric amplifiers (NOPAs) that generate two independently tunable beams. After compression, both beams can be frequency-doubled in a BBO crystal (only shown for one beam). The pulse length is characterized by an autocorrelator (AC). Finally, both beams are collinearly focused onto the sample within the PEEM under an angle of 65° relative to the surface normal. The temporal delay between both pulses is adjusted via a motorized delay stage.

and the other part is used for second- and third-harmonic generation (SHG, THG). The generated white light serves to seed both parametric amplification processes within two beta-barium borate (BBO) crystals, which are pumped by the generated SHG and THG beams, respectively. By adjusting the temporal delay between the pump pulses and the chirped white light, the output wavelength is tunable from 440 to 990 nm for the THG pumped beam and between 620 and 990 nm for the SHG pumped beam [26]. The configuration as *noncollinear* OPAs (optical parametric amplifiers) allows the shortening of the pulses by fused silica prism compressors (Figure 2) to typical pulse lengths in the range of 20–30 fs in the central spectral range at typical pulse energies between 75 and 200 nJ.

In the PEEM experiments shown here, the NOPA output of the THG pumped beam is frequency doubled in an additional BBO crystal and subsequently compressed in a third prism compressor. As the pulse energy of the second NOPA output IR beam is typically higher (150–200 nJ), it can also be frequency doubled within a separate BBO crystal, which has not been used here. Instead, this beam passes an automated linear translation stage to adjust the temporal delay between the two different beams. The characterization of the laser pulses is based on the autocorrelation of the IR pulses and the cross-correlation (CC) between the UV and IR pulses, which is used for the optimization of all prism compressors. Finally, the UV and IR beams are superimposed and collinearly focused through a MgF viewport onto the sample, which is positioned in the PEEM. The laser incidence angle is fixed to a polar angle of 65° due to the PEEM extractor geometry. Unless otherwise stated, the incident beam is p-polarized. The photoelectrons from the sample are accelerated by an extractor voltage of 10–15 kV into the PEEM (IS-PEEM**; FOCUS GmbH, Huenstetten, Germany) and pass several deflection and stigmator units, and two projective lenses for magnification [27]. The electron distribution after amplification in a multichannel plate is imaged on a fluorescence screen and digitized by a charge-coupled-device camera. The nominal resolution of the instrument is 40 nm, and typical field of views (FOVs) have diameters between 15 and 200 μm.

All experiments have been performed under UHV conditions at a base pressure of 10^{-10} mbar. The $BaTiO_3(001)$ surface has been prepared by mild Ar^+ sputtering, annealing to 1,000 K in 1×10^{-5} mbar O_2, and final flashing to 1,370 K in UHV. The long-range order of the surface has been verified by low-energy electron diffraction (LEED), which reveals a sharp (1×1) pattern. The correct $BaTiO_3$ composition after sample preparation has been checked by *in situ* X-ray photoemission (XPS). The second Ag(001) sample has been cleaned by several cycles of Ar^+ sputtering and subsequent annealing to approximately 680 K, leading to a well-prepared surface, as derived from the sharp LEED pattern and XPS.

Results and discussion

Imaging of the ferroelectric domains of $BaTiO_3$(001)

Figure 3(a) depicts a sequence of PEEM images of the clean $BaTiO_3(001) - (1 \times 1)$ surface at room temperature with an FOV of 150 μm for a laser photon energy of 4.28 eV. The imaged regions have been laterally shifted to obtain partly overlapping PEEM images of adjacent sample areas. In all PEEM images, stripelike patterns that we assign to different ferroelectric domains are observable. The marked PEEM image (red circle) shows a straight domain pattern aligned in the [100] high-symmetry direction with alternating domains, with widths of approximately (6.3 ± 1.4) μm and (7.9 ± 1.5) μm, respectively. The difference in photoemission intensity I_a and I_c of both domains, which is defining the contrast in the PEEM image, can be quantified by the photoemission asymmetry A between both domains as defined by

$$A = \frac{I_a - I_c}{I_a + I_c}.$$

For the marked PEEM image Figure 3(a) (left side), a strong photoemission asymmetry of $(38 \pm 2)\%$ is found.

Furthermore, Figure 3(a) clearly shows a change in the domain pattern for subsequent images when proceeding from the left to the right side. The stripelike domain pattern on the right side of Figure 3(a) shows a different contrast with an asymmetry of $(-22 \pm 2)\%$. As mentioned previously, the strict orientation of the domain walls in [100] direction strongly suggests an arrangement of alternating a and c domains. Within the full sequence of images in Figure 3(a), three different intensity levels can be distinguished. While the

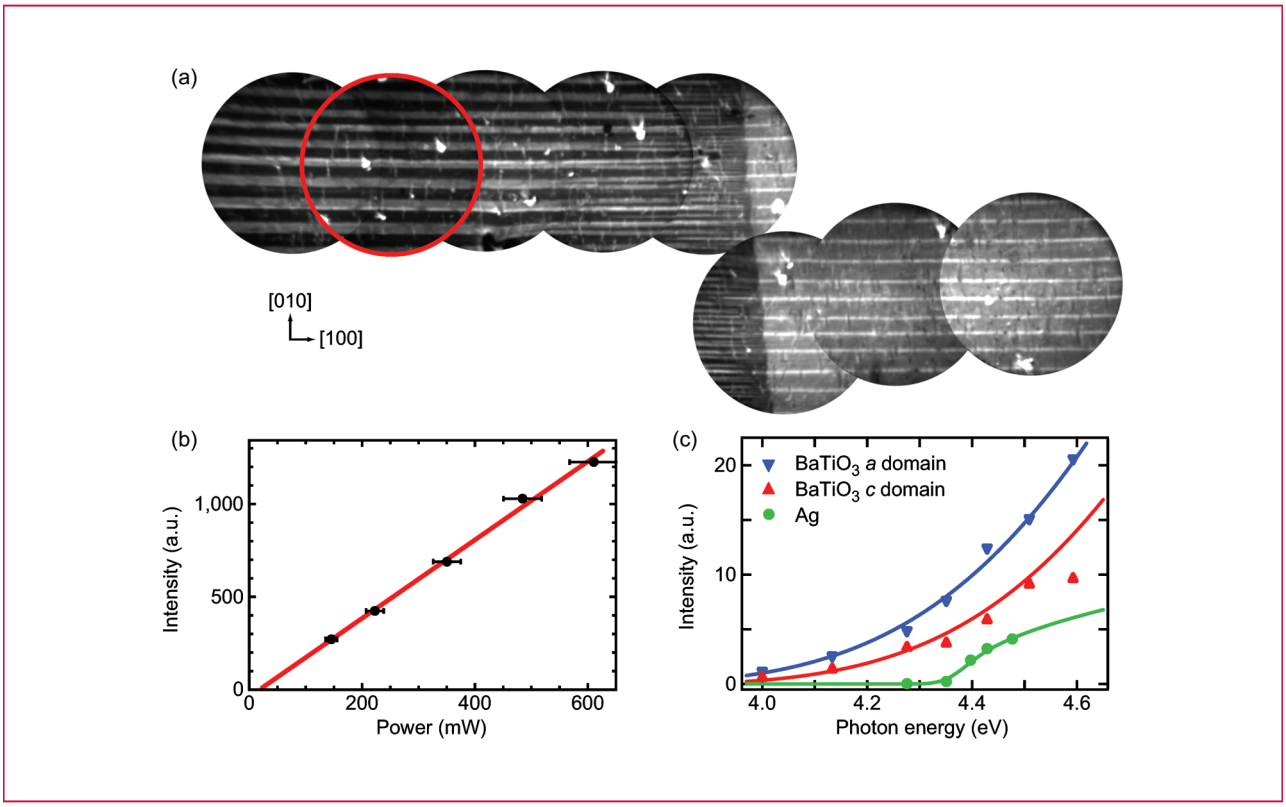

Figure 3

PEEM images and intensities. (a) PEEM images of adjacent sample areas showing the transition from an a–c^- domain configuration in the upper left to an a–c^+ domain configuration in the lower right (FOV = 150 μm each and a photon energy of 4.28 eV). (b) Average PEEM intensity as a function of the exciting laser light intensity at $h\nu = 4.35$ eV. (c) Normalized PEEM intensity in the photoemission onset for the a and c^- domains as a function of the photon energy of the laser light. The solid line shows a square-root-like onset for each domain (with $E_0 = 4.73$ and 4.84 eV) with a Gaussian broadening of 940 meV. Additionally, the threshold photoemission intensity for a bare Ag(001) surface is shown, which is described by an onset of $E_0 = 4.37$ eV and a Gaussian broadening of 70 meV (a.u.: arbitrary units).

left part shows virtually black and gray domains, the right part reveals almost white and also gray domains. From this observation, the gray-appearing domains are assigned to the a domains, whereas the brighter and darker areas are the c domains of opposite polarization direction. In the following, we consider the darkest domains as c^- and the brightest domains as c^+.

A prominent feature of Figure 3(a) is this abrupt almost vertical transition between both ferroelectric domain configurations. If one follows the a–c^- domain pattern starting from the left of Figure 3(a), one notices in the fourth image a splitting of each gray domain into two gray domains with a black domain in between. A further splitting into four gray domains is visible in the region of the fifth image. In parts of the sixth PEEM image, there are indications of a further splitting until the abrupt transition to the new a–c^+ domain configuration becomes more favorable. As the 90° a–c wall displacement depends strongly on strains within the crystal, the observed transition is proposed to be strain driven [28].

Figure 3(b) depicts the average PEEM image intensity for a photon energy of 4.35 eV as a function of the exciting UV laser power. The observed linear dependence of the photoemission signal on the number of photons per time reveals that one-photon photoemission contributes dominantly to image formation at this photon energy. The normalized intensity of individual a and c^- domains is shown in **Figure 3(c)** as a function of the photon energy, marked as triangles pointing down and up, respectively. As described in Figure 3(a) for a fixed photon energy of 4.28 eV, the a domains show a significantly higher intensity than the c^- domains. This holds for all photon energies, and both curves can be converted into each other by a shift on the energy axis. From additional wavelength-dependent measurements (not shown here), the photoemission onset of $BaTiO_3$ is determined to be 3.8 eV, which is also in line

with the data in Figure 3(c). However, this is in clear contrast to predictions from band calculations for an ideal crystal [29]. This seeming contradiction might be explained by the preparation-induced doping of the used $BaTiO_3$ crystal via formation of oxygen vacancies. A mild reduction of the $BaTiO_3$ crystal is necessary in order to obtain a conductive sample enabling photoemission experiments. Oxygen vacancies will pin the position of the Fermi level away from its position for a defect-free crystal (band gap center). This is supported by UV photoemission spectroscopy (UPS), which reveals a strong dependence of the $BaTiO_3$ work function on the reduction-oxidation state [30].

In the energy and angle integrating experiment of Figure 3(c), for description of the threshold photoemission one has to take into account the density of the photoemission initial states (DOS), a possible energy dependence of the photoemission matrix elements, and the density of accessible final states. For simplicity, we assume constant matrix elements in the photon energy range discussed here. In the following, a qualitative description of the threshold photoemission in the PEEM experiment will be derived using the example of Ag(001). Afterwards, this model will be adopted to describe the presented $BaTiO_3$ data. The DOS of the Ag bulk *sp*-band varies only slowly in the vicinity of the Fermi energy, which is the relevant energy region here, whereas the number of accessible states will increase strongly with energy above the threshold. Due to the low initial electron kinetic energies, the surface transmission probability into the vacuum plays an important role for direct photoelectrons, as well as for elastically and inelastically scattered electrons. Berglund et al. and Pontius et al. calculated this so-called escape function for silver surfaces. The escape function increases with increasing energy similar to a square-root-like behavior [31, 32]. To describe the photon-energy-dependent electron yield, one has to integrate over all these processes, which is beyond the scope of this paper, and to convolve the result with an experimental Gaussian broadening, which accounts for the finite energy resolution, the bandwidth of the fs laser pulses, and the inhomogeneities of the sample. We approximate the experimental data (marker) in Figure 3(c) in a simplified model by a convolution of a square root function $\sqrt{E - E_0}$ and a Gaussian. Here, E denotes the energy, and E_0 denotes the onset of this square root function. The photoemission onset data for Ag(001) is also shown in Figure 3(c) and can be described by this model with a broadening of 70 meV. This broadening can be fully explained by the spectral width of the laser pulses of (70 $\pm$ 10) meV. The inflection point for the Ag(001) data is located at (4.39 $\pm$ 0.05) eV, which is in good agreement with the literature value of the Ag(001) work function [33]. In contrast to the Ag(001) data, the onset is much wider for both $BaTiO_3$ domains. The data are compatible with a broadening of 940 meV and a band onset E_0 of 4.73 and 4.84 eV. The additional broadening as compared with Ag(001) is large and not understood so far. A possible explanation might be found in the local variations of the oxygen vacancy concentration. It has been reported that the work function as determined by UPS depends significantly on the reduction–oxidation state of the sample, which corresponds to the oxygen vacancy concentration. Local variations of the vacancy concentration on a length scale significantly smaller than the ferroelectric domain sizes would lead to locally different onsets, which can explain the observed broadening within the ferroelectric domains. Since it is not expected that these local differences in the density of oxygen defects are distributed heterogeneously on different domain types, the energy shift between both data sets of about 110 meV might represent the difference of the surface potential between the *a* and c^- domains. The observed difference is on the order of the value measured by Kalinin et al. under ambient conditions where screening of the polarization charge plays an important role [34].

Two-photon PEEM of the first image potential state on Ag(001)

Whereas, in the previous section, PEEM data based on one-photon photoemission processes have been presented, the use of two different fs laser pulses for two-photon photoemission (2PPE) allows for time-resolved PEEM in a pump-probe setup. In the following, we demonstrate the high temporal resolution of PEEM based on UV pump and IR probe experiments on the electron dynamics of image potential states of the Ag(001) surface using the laser setup shown in Figure 2. An Ag(001) surface is illuminated by UV laser pulses of a photon energy of 3.95 eV, which corresponds to the energy position of the first image potential state with respect to the Fermi energy at the $\overline{\Gamma}$-point. A second IR pulse of 1.65 eV is used to probe the population of the image potential state by photoemission above the vacuum level. The photoelectrons are collected by the PEEM. Only near the temporal overlap between pump and probe beam does PEEM show significant intensity. Since a homogeneous Ag(001) surface is used, the photoemission intensity within a PEEM image is constant and structureless (not shown here). **Figure 4** shows this PEEM intensity (marked as red triangles) after subtraction of a constant background as a function of the temporal delay between the UV and IR laser pulses on a logarithmic scale. The data show a fast increase over almost two orders of magnitude for negative delay times (IR pulse first) and a significant slower decay for positive delays (UV pulse first). This asymmetry proves that the photoelectrons originate from electronic states that are populated by the UV pump pulse and are probed by the IR pulses. For delay times longer than 50 fs, the PEEM intensities are dominated by an exponential decay, as can be seen by the linear decrease on the logarithmic scale. A modeling that takes the finite pulse length of both laser

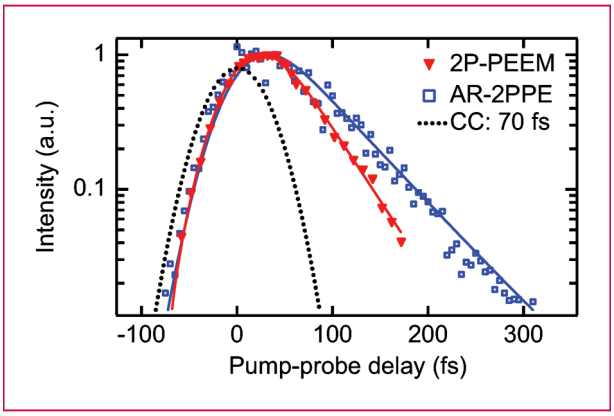

Figure 4

Logarithmic 2PPE intensity of the first image potential state of a bare Ag(001) surface measured by PEEM (solid red triangles) and by angle-resolved 2PPE at the $\overline{\Gamma}$-point (open blue squares) using the same laser setup. The solid lines represent the fits to the respective data set with a convolution of a single exponential decay and the Gaussian-shaped cross-correlation (CC) between pump and probe beam (a.u.: arbitrary units).

pulses with a cross-correlation of 70 fs into account (dashed black line in Figure 4) describes the data fully (red solid line). It allows determining the apparent lifetime to (40 ± 10) fs. For comparison, the normal-emission data of an angle- and energy-resolved 2PPE experiment on the same Ag(001) surface are shown as blue squares. These data have been measured with the same laser setup but in a second UHV chamber that is equipped with a hemispherical 2-D electron analyzer ((Phoibos 150**; SPECS GmbH, Berlin, Germany). The energy-resolved data in Figure 4 show the identical onset and an exponential decay that corresponds to a lifetime of (57 ± 10) fs. Additional data (not shown here) allow the identification of the photoemission process [35]: The UV pulse populates the first image potential state, which is located 540 meV below the vacuum level [33, 35]. By the IR probe beam, the electrons are then photoemitted. The observed lifetime is in good agreement with experimentally and theoretically derived values [36, 37]; details can be found elsewhere [35].

Whereas the overall agreement between 2P-PEEM and 2PPE experiments is quite good, there is a clearly shorter lifetime observed in PEEM. In contrast to the angle- and energy-resolved 2PPE experiment, in PEEM, photoelectrons of all kinetic energies are collected over a wide range of photoemission angles and contribute to the measured signal. Since the work function of Ag(001) is approximately 4.44 eV, a pump pulse of 3.95 eV should populate the first image potential with electrons from the Fermi level only in a narrow momentum range around the $\overline{\Gamma}$-point. However, as the lifetime of the electrons in the image potential states depends strongly on their parallel momentum, this will contribute to a shorter averaged lifetime [35, 38]. An additional signal from UV-pumped short-lived Ag bulk states at large parallel momentum far from the $\overline{\Gamma}$-point seems possible based on the Ag(001) band structure (see, e.g., [39]) and might contribute to the PEEM signal. Hence, we propose that, in the 2P-PEEM experiment, the unoccupied Ag bulk states are co-excited and contribute in addition to the first image potential state to the apparent lifetime. This results in a reduced effective lifetime as compared with the lifetime of the first image potential state.

Conclusion

Three different ferroelectric domain types of $BaTiO_3(001)$ have been imaged by PEEM, using a widely tunable laser system. Photon-energy-dependent measurements close to the photoemission threshold have revealed an energy shift between the photoemission onsets of the a and c^- domains of approximately 110 meV. In similar experiments, for Ag(001), a work function of (4.39 ± 0.05) eV has been found to be in agreement with literature values. In a pump-probe PEEM experiment, in which the first image potential state of Ag(001) is excited, an apparent lifetime of approximately 40 fs has been derived from analysis of the PEEM intensities. Angle- and energy-resolved 2PPE data measured with the same laser setup have revealed a lifetime of (57 ± 10) fs according to literature. The observed difference has been discussed in terms of co-excitation of bulk states with larger parallel momentum.

Acknowledgments

This work was supported by the Deutsche Forschungsgemeinschaft through the Sonderforschungsbereich SFB-762 “Functional Oxidic Interfaces.” The authors would like to thank Ralf Kulla for technical support.

**Trademark, service mark, or registered trademark of Clark-MXR or Focus GmbH in the United States, other countries, or both.

References

1. J. Stöhr, Y. Wu, B. D. Hermsmeier, M. G. Samant, G. R. Harp, S. Koranda, D. Dunham, and B. P. Tonner, “Element-specific magnetic microscopy with circularly polarized X-rays,” *Science*, vol. 259, no. 5095, pp. 658–661, Jan. 1993.
2. O. Schmidt, G. H. Fecher, Y. Hwu, and G. Schönhense, “The spatial distribution of non-linear effects in multiphoton photoemission from metallic adsorbates on Si(111),” *Surf. Sci.*, vol. 482–485, pp. 687–692, Jun. 2001.
3. O. Schmidt, M. Bauer, C. Wiemann, R. Porath, M. Scharte, O. Andreyev, G. Schönhense, and M. Aeschlimann, “Time-resolved two photon photoemission electron microscopy,” *Appl. Phys. B, Lasers Opt.*, vol. 74, no. 3, pp. 223–227, Mar. 2002.
4. A. Kubo, K. Onda, H. Petek, Z. J. Sun, Y. S. Jung, and H. K. Kim, “Ferntosecond imaging of surface plasmon dynamics in a nanostructured silver film,” *Nano Lett.*, vol. 5, no. 6, pp. 1123–1127, 2005.
5. M. Bauer, C. Wiemann, J. Lange, D. Bayer, M. Rohmer, and M. Aeschlimann, “Phase propagation of localized surface plasmons probed by time-resolved photoemission electron

microscopy," *Appl. Phys. A, Solids Surf.*, vol. 88, no. 3, pp. 473–480, Aug. 2007.
6. F.-J. Meyer zu Heringdorf, L. I. Chelaru, S. Möllenbeck, D. Thien, and M. Horn-von Hoegen, "Femtosecond photoemission microscopy," *Surf. Sci.*, vol. 601, no. 20, pp. 4700–4705, Oct. 2007.
7. A. Kubo, Y. S. Jung, H. K. Kim, and H. Petek, "Femtosecond microscopy of localized and propagating surface plasmons in silver gratings," *J. Phys. B, Atom. Mol. Opt. Phys.*, vol. 40, no. 11, pp. S259–S272, Jun. 2007.
8. D. Bayer, C. Wiemann, O. Gaier, M. Bauer, and M. Aeschlimann, "Time-resolved 2PPE and time-resolved PEEM as a probe of LSP's in silver nanoparticles," *J. Nanomater.*, vol. 2008, pp. 249514-1–249514-11, 2008.
9. A. Oelsner, M. Rohmer, C. Schneider, D. Bayer, G. Schönhense, and M. Aeschlimann, "Time- and energy resolved photoemission electron microscopy-imaging of photoelectron time-of-flight analysis by means of pulsed excitations," *J. Electron Spectrosc. Related Phenom.*, vol. 178/179, pp. 317–330, May 2010.
10. M. Rohmer, M. Bauer, T. Leissner, C. Schneider, A. Fischer, G. Niedner-Schatteburg, B. von Issendorff, and M. Aeschlimann, "Time-resolved photoelectron nano-spectroscopy of individual silver particles: Perspectives and limitations," *Phys. Stat. Sol. B, Basic Solid State Phys.*, vol. 247, no. 5, pp. 1132–1138, May 2010.
11. K. Fukumoto, T. Matsushita, H. Osawa, T. Nakamura, T. Muro, K. Arai, T. Kimura, Y. Otani, and T. Kinoshita, "Construction and development of a time-resolved X-ray magnetic circular dichroism-photoelectron emission microscopy system using femtosecond laser pulses at BL25SU SPring-8," *Rev. Sci. Instrum.*, vol. 79, no. 6, p. 063903, Jun. 2008.
12. J. Miguel, M. Bernien, D. Bayer, J. Sanchez-Barriga, F. Kronast, M. Aeschlimann, H. A. Dürr, and W. Kuch, "A new sample holder for laser-excited pump-probe magnetic measurements on a Focus photoelectron emission microscope," *Rev. Sci. Instrum.*, vol. 79, no. 3, p. 033702, Mar. 2008.
13. K. Hild, J. Maul, T. Meng, M. Kallmayer, G. Schönhense, H. J. Elmers, R. Ramos, S. K. Arora, and I. V. Shvets, "Optical magnetic circular dichroism in threshold photoemission from a magnetite thin film," *J. Phys. Condens. Matter*, vol. 20, no. 23, pp. 235218, Jun. 2008.
14. T. Nakagawa, K. Watanabe, Y. Matsumoto, and T. Yokoyama, "Magnetic circular dichroism photoemission electron microscopy using laser and threshold photoemission," *J. Phys. Condens. Matter*, vol. 21, no. 31, p. 314010, Aug. 2009.
15. T. Nakagawa and T. Yokoyama, "Magnetic circular dichroism near the fermi level," *Phys. Rev. Lett.*, vol. 96, no. 23, p. 237402, Jun. 2006.
16. D. Thien, P. Kury, M. Horn-von Hoegen, F.-J. Meyer zu Heringdorf, J. van Heys, M. Lindenblatt, and E. Pehlke, "Domain sensitive contrast in photoelectron emission microscopy," *Phys. Rev. Lett.*, vol. 99, no. 19, p. 196102, Nov. 2007.
17. B. M. Wul and I. Goldman, *Comptes Rendu (USSR)*, vol. 46, pp. 139, 1945.
18. A. von Hippel, R. G. Breckenridge, F. G. Chesley, and L. Tisza, "High dielectric constant ceramics," *Ind. Eng. Chem.*, vol. 38, no. 11, pp. 1097–1109, 1946.
19. W. J. Merz, "The electric and optical behavior of $BaTiO_3$ single-domain crystals," *Phys. Rev.*, vol. 76, no. 8, pp. 1221–1225, Oct. 1949.
20. E. Fuchs and W. Liesk, "Elektronenmikroskopische Beobachtung von Domänenkonfigurationen und von Umpolarisationsvorgängen in dünnen $BaTiO_3$-Einkristallen," *J. Phys. Chem. Solids*, vol. 25, no. 8, pp. 845–848, Aug. 1964.
21. R. Le Bihan, "Observation de la surface de cristaux de titanate de baryum au microscope à photoémission," *Comptes Rendus Hebdomadaires Des Seances De L' Acad. Sci. Ser. B*, vol. 275, no. 1, pp. 29–32, 1972.
22. C. Hagendorf, K.-M. Schindler, T. Doege, and H. Neddermeyer, "Surface physical studies of poly- and single-crystalline $BaTiO_3$," *Appl. Surf. Sci.*, vol. 142, no. 1–4, pp. 106–113, Apr. 1999.
23. C. Hagendorf, K.-M. Schindler, T. Doege, and H. Neddermeyer, "An STM, XPS and LEED investigation of the $BaTiO_3(111)$ surface," *Surf. Sci.*, vol. 402, no. 1–3, pp. 581–585, May 1998.
24. Y. H. Hu, H. M. Chan, X. W. Zhang, and M. P. Harmer, "Scanning electron-microscopy and transmission electron-microscopy study of ferroelectric domains in doped $BaTiO_3$," *J. Amer. Ceram. Soc.*, vol. 69, no. 8, pp. 594–602, Aug. 1986.
25. M. Fechner, S. Ostanin, and I. Mertig, "Effect of the surface polarization in polar perovskites studied from first principles," *Phys. Rev. B*, vol. 77, no. 9, p. 094112, Mar. 2008.
26. C. Homann, C. Schriever, P. Baum, and E. Riedle, "Octave wide tunable UV-pumped NOPA: Pulses down to 20 fs at 0.5 MHz repetition rate," *Opt. Exp.*, vol. 16, no. 8, pp. 5746–5756, Apr. 2008.
27. W. Swiech, G. Fecher, C. Ziethen, O. Schmidt, G. Schönhense, K. Grzelakowski, C. M. Schneider, R. Frömter, H. Oepen, and J. Kirschner, "Recent progress in photoemission microscopy with emphasis on chemical and magnetic sensitivity," *J. Electron Spectrosc. Related Phenom.*, vol. 84, no. 1–3, pp. 171–188, Mar. 1997.
28. E. A. Little, "Dynamic behavior of domain walls in barium titanate," *Phys. Rev.*, vol. 98, no. 4, pp. 978–984, May 1955.
29. A. Filippetti and N. A. Spaldin, "Strong-correlation effects in born effective charges," *Phys. Rev. B*, vol. 68, no. 4, p. 045111, Jul. 2003.
30. C. Hagendorf, "Oberflächenphysikalische Untersuchungen an ein- und polykristallinem $BaTiO_3$-Morphologie, atomare und elektronische Struktur," Ph.D. dissertation, Martin-Luther-Univ. Halle-Wittenberg, Halle, Germany, 2000.
31. C. N. Berglund and W. E. Spicer, "Photoemission studies of copper and silver—Experiment," *Phys. Rev. A, Gen. Phys.*, vol. 136, no. 4A, pp. 1044–1064, Nov. 1964.
32. N. Pontius, V. Sametoglu, and H. Petek, "Simulation of two-photon photoemission from the bulk sp-bands of Ag(111)," *Phys. Rev. B*, vol. 72, no. 11, p. 115105, Sep. 2005.
33. S. Schuppler, N. Fischer, T. Fauster, and W. Steinmann, "Bichromatic 2-photon photoemission spectroscopy of image potential states on Ag(100)," *Appl. Phys. A, Solids Surf.*, vol. 51, no. 4, pp. 322–326, Oct. 1990.
34. S. V. Kalinin and D. A. Bonnell, "Local potential and polarization screening on ferroelectric surfaces," *Phys. Rev. B*, vol. 63, no. 12, p. 125411, Mar. 2001.
35. K. Duncker, M. Kiel, and W. Widdra, "Parallel-momentum-resolved lifetimes of image potential states at a Ag(001) surface—Direct measurement with time-resolved 2PPE," 2011, in preparation.
36. I. L. Shumay, U. Höfer, U. Thomann, W. Wallauer, and T. Fauster, "Lifetimes of image-potential states on Cu(100) and Ag(100) measured by femtosecond time-resolved two-photon photoemission," *Phys. Rev. B*, vol. 58, no. 20, pp. 13,974–13,981, Nov. 1998.
37. E. V. Chulkov, V. M. Silkin, and P. M. Echenique, "Image potential states on lithium, copper and silver surfaces," *Surf. Sci.*, vol. 391, no. 1–3, pp. L1217–L1223, Nov. 1997.
38. W. Berthold, U. Höfer, P. Feulner, E. V. Chulkov, V. M. Silkin, and P. M. Echenique, "Momentum-resolved lifetimes of image-potential states on Cu(100)," *Phys. Rev. Lett.*, vol. 88, no. 5, p. 056805, Feb. 2002.
39. W. Altmann, V. Dose, and A. Goldmann, "Momentum-resolved Bremsstrahlung Isochromat Spectroscopy of Silver surfaces," *Zeitschrift für Phys. B, Condens. Matter*, vol. 65, no. 2, pp. 171–180, Jun. 1986.

Received October 1, 2010; accepted for publication February 14, 2011

Anke Höfer *Institute of Physics, Martin-Luther-Universität Halle-Wittenberg, 06120 Halle, Germany (anke.hoefer@physik.uni-halle.de)*.

Klaus Duncker *Institute of Physics, Martin-Luther-Universität Halle-Wittenberg, 06120 Halle, Germany (klaus.duncker@physik.uni-halle.de)*.

Mario Kiel *Institute of Physics, Martin-Luther-Universität Halle-Wittenberg, 06120 Halle, Germany (mario.kiel@physik.uni-halle.de)*.

Stefan Förster *Institute of Physics, Martin-Luther-Universität Halle-Wittenberg, 06120 Halle, Germany (stefan.foerster@physik.uni-halle.de)*.

Wolf Widdra *Institute of Physics, Martin-Luther-Universität Halle-Wittenberg, 06120 Halle, Germany (wolf.widdra@physik.uni-halle.de)*.